Energies **2015**, *8*, 6898-6909; doi:10.3390/en8076898

OPEN ACCESS

energies

ISSN 1996-1073

www.mdpi.com/journal/energies

Article

The improved Hydrogen Storage Performances of the Multi-Component Composite: $2Mg(NH_2)_2$–$3LiH$–$LiBH_4$

Han Wang [1,2], Hujun Cao [1], Guotao Wu [1,*], Teng He [1] and Ping Chen [1]

[1] Dalian National Laboratory for Clean Energy, Dalian Institute of Chemical Physics, Chinese Academy of Sciences, Dalian 116023, China; E-Mails: wanghan@dicp.ac.cn (H.W.); caohujun@gmail.com (H.C.); heteng@dicp.ac.cn (T.H.); pchen@dicp.ac.cn (P.C.)

[2] Graduate School of the Chinese Academy of Sciences, Beijing 100049, China

* Author to whom correspondence should be addressed; E-Mail: wgt@dicp.ac.cn; Tel./Fax: +86-411-8437-9583.

Academic Editor: Craig M. Jensen

Received: 25 May 2015 / Accepted: 30 June 2015 / Published: 10 July 2015

Abstract: $2Mg(NH_2)_2$–$3LiH$–$LiBH_4$ composite exhibits an improved kinetic and thermodynamic properties in hydrogen storage in comparison with $2Mg(NH_2)_2$–$3LiH$. The peak temperature of hydrogen desorption drops about 10 K and the peak width shrinks about 50 K compared with the neat $2Mg(NH_2)_2$–$3LiH$. Its isothermal dehydrogenation and re-hydrogenation rates are respectively 2 times and 18 times as fast as those of $2Mg(NH_2)_2$–$3LiH$. A slope desorption region with higher equilibrium pressure is observed. By means of X-ray diffraction (XRD), Fourier transform infrared spectroscopy (FTIR) and nuclear magnetic resonance (NMR) analyses, the existence of Li_2BNH_6 is identified and its roles in kinetic and thermodynamic enhancement are discussed.

Keywords: hydrogen storage; amide-hydride system; sorption kinetics; Li_2BNH_6

1. Introduction

Owing to the worldwide demand for the renewable energy sources, hydrogen will be an ideal energy carrier if it can be stored safely, efficiently and conveniently [1]. Numerous solid-state hydrogen storage materials have been developed to store hydrogen in an energy or volume efficient way [2]. Complex hydrides, e.g., alanates [3–5], borohydrides [6–8], and amide-hydride systems [9–20] are promising to

fulfill the on-board hydrogen storage requirements. In particular, a number of amide–hydride systems, such as Li–N–H [10], Li–Mg–N–H [11,13,17–20], Li–Ca–N–H [14], Li–Al–N–H [15], Mg–N–H [12], Ca–N–H [16], and so on [9,14,21,22] have been investigated since 2002. As for the Li–Mg–N–H system, $Li_2Mg(NH)_2$ can be obtained by releasing hydrogen from MgH_2–$2LiNH_2$ composite or $Mg(NH_2)_2$–2LiH composite, which has attracted considerable attention due to its favorable thermodynamics ($\Delta H \approx 40$ kJ/mol-H_2), relatively high hydrogen capacity (5.6 wt%) and good reversibility.

Hydrogenation/dehydrogenation processes of $Li_2Mg(NH)_2$ were probed under the pressure composition isotherms conditions by *ex-situ* X-ray diffraction (XRD) [17] and *in-situ* neutron measurements [23]. During the hydrogenation process, $Li_2Mg(NH)_2$ is first converted to $Li_2Mg_2(NH)_3$, $LiNH_2$ and LiH at a low pressure slope, and then form $Mg(NH_2)_2$ and 2LiH at the high pressure plateau. In the dehydrogenation, $Mg(NH_2)_2$ and 2LiH take the reverse reaction route and go back to $Li_2Mg(NH)_2$.

The reactions can be described as follows:

$$2Mg(NH_2)_2 + 3LiH \rightleftharpoons Li_2Mg_2(NH)_3 + LiNH_2 + 2H_2 \quad (1)$$

$$Li_2Mg_2(NH)_3 + LiNH_2 + LiH \rightleftharpoons Li_2Mg(NH)_2 + 2H_2 \quad (2)$$

Considerable works have been carried out to lower down the operating temperature and improve the dehydrogenation kinetics of $Mg(NH_2)_2$–2LiH composite by doping additives, such as alkali metal compounds [24–27] and metal borohydrides [28,29]. The addition of KH significantly reduced the operating temperature from *ca.* 523 to 380 K, while the equilibrium pressure was *ca.* 0.2 MPa. Rb based compounds were found to be more effective for improving the kinetic properties of $Mg(NH_2)_2$–2LiH composite than the potassium based additives, and the active species was identified to be RbH [24,30]. Yang *et al.* [31] reported that a multi-component composite of $LiNH_2$, MgH_2 and $LiBH_4$ with a molar ratio of 2:1:1 exhibited enhanced low-temperature desorption kinetics and a significant reduction in ammonia liberations. As a kind of self-catalyzing hydrogen storage material, $LiBH_4$ catalyzed the dehydrogenation of $2LiNH_2$–MgH_2 composite to form $Li_2Mg(NH)_2$, furthermore $Li_2Mg(NH)_2$ could react with $LiBH_4$ to release more hydrogen. Following this work, Hu *et al.* [29] doped 10 mol% $LiBH_4$ in $Mg(NH_2)_2$–2LiH composite and found the doping of $LiBH_4$ not only improved the kinetics but also reduced the heat of dehydrogenation from 40 kJ/mol-H_2 of $Mg(NH_2)_2$–2LiH composite to 36.5 kJ/mol-H_2 of $Mg(NH_2)_2$–2LiH–$0.1LiBH_4$ composite. Other borohydrides, such as $Mg(BH_4)_2$ and $Ca(BH_4)_2$ [32–34], have similar effects as $LiBH_4$ in $Mg(NH_2)_2$–2LiH composite because they convert to $LiBH_4$ after a metathesis reaction. Li *et al.* [35] introduced 5 mol% LiBr to $2LiNH_2$–MgH_2 composite and found certain effects on its thermodynamics and kinetics. In Cao's recentwork [36], thermodynamic properties of the dehydrogenation of $2Mg(NH_2)_2$–3LiH composite were improved by stabilizing the dehydrogenated product, $LiNH_2$, in Reaction (1). $LiNH_2$ reacts with $LiBH_4$, LiI and LiBr exothermically and forms more stable compounds, *i.e.*, $Li_4(NH_2)_3BH_4$, $Li_3(NH_2)_2I$, and $Li_2(NH_2)Br$; the reactions are as follows:

$$2Mg(NH_2)_2 + 3LiH + 1/2LiI \rightleftharpoons Li_2Mg_2(NH)_3 + 1/2Li_3(NH_2)_2I + 3H_2 \quad (3)$$

$$2Mg(NH_2)_2 + 3LiH + LiBr \rightleftharpoons Li_2Mg_2(NH)_3 + Li_2NH_2Br + 3H_2 \quad (4)$$

$$2Mg(NH_2)_2 + 3LiH + 1/3LiBH_4 \rightleftharpoons Li_2Mg_2(NH)_3 + 1/3Li_4BN_3H_{10} + 3H_2 \quad (5)$$

The additions of $LiBH_4$, LiI and LiBr noticeably reduced the heat of dehydrogenation from 40 kJ/mol-H_2 of $2Mg(NH_2)_2$–3LiH composite to 35.8, 33.3 and 31.9 kJ/mol-H_2, respectively, which suggests that hydrogen release at 0.1 MPa equilibrium pressure can be thermodynamically allowed at 337, 333 and 320 K, respectively. Quaternary complex hydrides, such as Li_2BNH_6 [37] and $Li_4BN_3H_{10}$ [38], were found by ball milling or heating the mixtures of $LiNH_2$ and $LiBH_4$ with corresponding molar ratios. If with more $LiBH_4$ to facilitate the formation of Li_2BNH_6, Reaction (5) can be rewritten as Reaction (6):

$$2Mg(NH_2)_2 + 3LiH + LiBH_4 \rightleftharpoons Li_2Mg_2(NH)_3 + Li_2BNH_6 + 3H_2 \quad (6)$$

Herein we report the modification of $2Mg(NH_2)_2$–3LiH system by adding a different ratio of $LiBH_4$. The dehydrogenation and re-hydrogenation performances of $Mg(NH_2)_2$–2LiH–1$LiBH_4$ composite were investigated by Thermogravimetry coupled differential thermal analysis (TG-DTA) measurement, temperature programmed desorption-mass spectroscopy (TPD-MS), isothermal volumetric release, and soak. We found that the increase in the amount of $LiBH_4$ improved the kinetics of $2Mg(NH_2)_2$–3LiH composite.

An interesting phenomenon was observed that there was a higher pressure slope in pressure composition isotherm (PCI) measurements of $2Mg(NH_2)_2$–3LiH–$LiBH_4$ composite than $2Mg(NH_2)_2$–3LiH–1/3$LiBH_4$ composite [36], which reveals the change of thermodynamic properties. Samples at this stage were analyzed by means of X-ray diffraction (XRD), Fourier transform infrared spectroscopy (FTIR), and magic angle spinning nuclear magnetic resonance (MAS NMR).

2. Results and Discussion

2.1. The hydrogen Desorption Properties of $2Mg(NH_2)_2$–3LiH–$LiBH_4$ Composite

TG curve of $2Mg(NH_2)_2$–3LiH–$LiBH_4$ composite (T_2) is shown in Figure 1a. The thermal desorption of this sample exhibits two main steps, one is from 400 K to 450 K and the other is from 475 K to 575 K. The weight losses of the first step and the second step are 3.63 wt% and 6.24 wt%, respectively. Moreover, the first-step weight loss is near the theoretical loss of H_2 (3.7 wt%) deduced from Reaction (6).

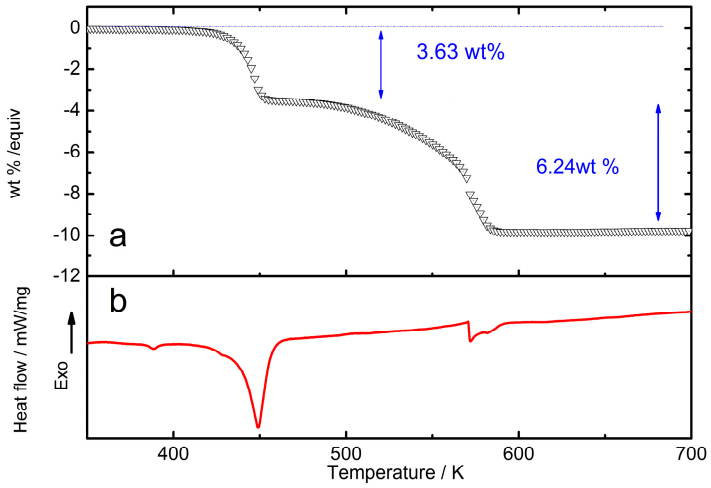

Figure 1. TG-DTA curves of $2Mg(NH_2)_2$–3LiH–$LiBH_4$ composite (T_2) (**a**) TG and (**b**) DTA.

The DTA curve of T_2 gives two main endothermic signals corresponding to the two desorption steps in TG curve. The small endothermic peak in Figure 1 at 363 K can be assigned to the phase transformation of $LiBH_4$ in starting materials.

The kinetic desorption behaviors of $2Mg(NH_2)_2$–3LiH (T_p) and $2Mg(NH_2)_2$–3LiH–$LiBH_4$ (T_2) composites were investigated by TPD-MS too. H_2 and NH_3 signals are shown in Figure 2a,b, respectively. As shown in Figure 2b, the byproduct ammonia can be effectively inhibited in T_2 sample during desorption process, and the two-step dehydrogenation of T_2 sample is corresponding to the result of TG. In the first dehydrogenation step of T_2 sample, 3.63 wt% hydrogen can be released according to the thermogravimetry analysis, which is near the weight loss of 3.7 wt% deduced from Reaction (6). The first dehydrogenation step of T_2 sample occurred at the temperature of 400 K, and finished at 460 K. The first dehydrogenation peak temperature of T_2 sample lowers *ca.*10 K compared with that of T_p sample (462 K), and the peak width shrinks *ca.* 50 K from that of T_p samples. Such a sharp dehydrogenation peak reflects a fast rate of dehydrogenation near the peak temperature. Furthermore, the dehydrogenation activation energies (E_a) of T_2 sample and T_p sample were determined by the Kissinger's method [36]. Through the calculation, the activation energy (E_a) of T_2 sample is 109 kJ/mol, which is lower than that of T_p (127 kJ/mol).

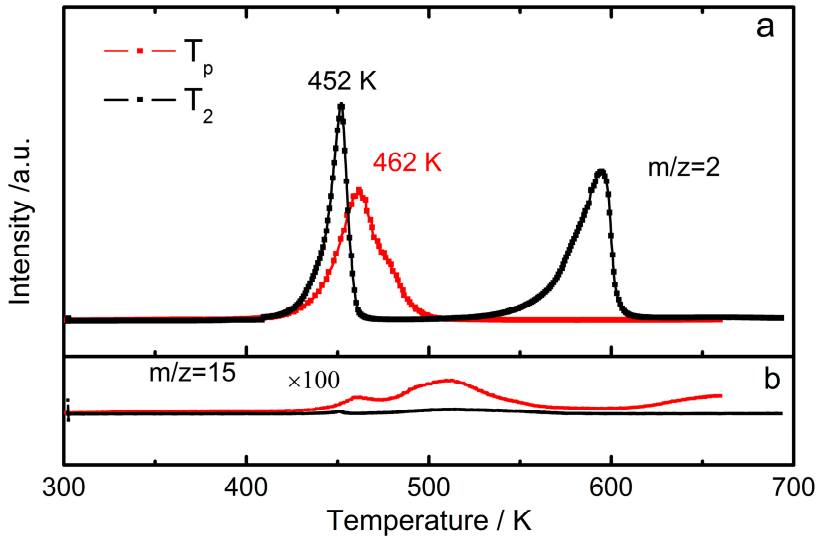

Figure 2. TPD-MS curves of $2Mg(NH_2)_2$–3LiH composite (T_p), and $2Mg(NH_2)_2$–3LiH–$LiBH_4$ composite (T_2): (**a**) H_2 signals and (**b**) NH_3 signals.

Isothermal dehydrogenation and re-hydrogenation of T_2 and T_p samples at 416 K were performed. Figure 3 (more detailed information is showed in Figure S1) shows that desorption and absorption kinetics of T_2 sample are accelerated remarkably in comparison with the T_p sample. In 100 min T_2 sample releases *ca.* 80% hydrogen, while T_p sample only releases 40% hydrogen, where the total amount of hydrogen is calculated according to Reaction (6) and Reaction (1), respectively. The tangent slopes of the initial linear parts also indicate that the dehydrogenation rate of the T_2 sample is *ca.* 2 times as fast as that of T_p sample. In the re-hydrogenation test, *ca.* 80% hydrogen can be charged back to T_2 sample within 50 min, while under the same condition, only *ca.* 20% hydrogen can be soaked in T_p sample. And the tangent slopes of the initial linear parts also show that T_2 is *ca.* 18 times as fast as that of the T_p sample.

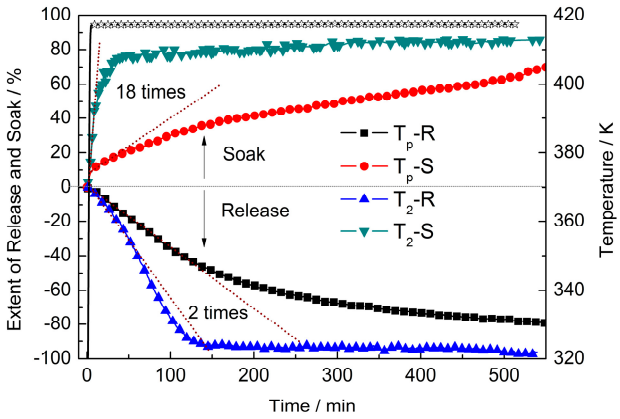

Figure 3. Isothermal hydrogen desorption and sorption of the $2Mg(NH_2)_2$–$3LiH$ composite (T_p), $2Mg(NH_2)_2$–$3LiH$–$LiBH_4$ composite (T_2) at 416 K under the pressure of 0.01 and 6 MPa, respectively.

XRD patterns of T_2 samples after dehydrogenation and re-hydrogenation at 460 K were collected for structural analyses. As shown in Figure 4a, the dehydrogenation products of T_2 sample are $Li_2Mg_2(NH)_3$ and $Li_4BN_3H_{10}$, which is somehow out of our initial expectation. Li_2BNH_6 has a hexagonal structure, and melts at ~365 K. $Li_4BN_3H_{10}$ has a body-centered cubic structure, and melts at ~465 K. Li_2BNH_6 is less stable than $Li_4BN_3H_{10}$ at temperatures above the melting temperature and decomposes to $Li_4BN_3H_{10}$ and $LiBH_4$ [39]. However, we did not observe crystalline $LiBH_4$ phase in XRD patterns in Figure 4a, which may become amorpous during this process. After the following re-hydrogenation, $Mg(NH_2)_2$ and LiH are regenarated and $Li_4BN_3H_{10}$ still remains (seen in Figure 4a). The melting of $Li_4BN_3H_{10}$ and/or Li_2BNH_6 may create a unique reaction environment, allowing interface reaction and mass transport of Reaction (1) to proceed at a faster rate [40]. Figure 4b shows the FTIR spectra of dehydrogenation and re-hydrogenation samples. The symmetric and asymmetric N–H stretching vibrations of $Li_4BN_3H_{10}$ are at 3243 and 3302 cm^{-1}, while the symmetric and asymmetric N–H stretching vibrations of $LiNH_2$ are at 3257 and 3310 cm^{-1}. Corresponding to the results of XRD characterization, the vibrations of $Li_4BN_3H_{10}$ can be found in the dehydrogenation and re-hydrogenation products of T_2 sample. Isothermal dehydrogenation/re-hydrogenation processes of T_2 sample are not fully reversible due to the kinetic and/or thermodynamic reasons. $Li_2Mg_2(NH)_3$ or MgNH is found in the re-hydrogenated sample, which exhibits the vibration at 3197 cm^{-1}.

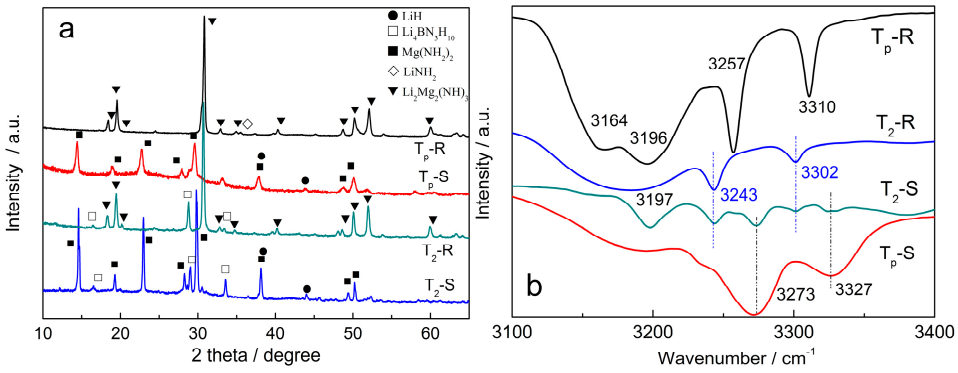

Figure 4. (**a**) XRD patterns and (**b**) FT-IR spectrum of $2Mg(NH_2)_2$–$3LiH$ (T_p) and $2Mg(NH_2)_2$–$3LiH$–$LiBH_4$ (T_2) samples release (R) and soak (S) at 460 K.

2.2. Pressure–Composition–Isotherm (PCI) Dehydrogenation at High Pressure

Pressure–Composition–Isotherm (PCI) dehydrogenation curves at 473 K of $2Mg(NH_2)_2$–3LiH (T_p), $2Mg(NH_2)_2$–3LiH–$LiBH_4$ (T_2) and $2Mg(NH_2)_2$–3LiH–1/3$LiBH_4$ (T_4) samples are shown in Figure 5. It can be seen that the equilibrium plateau pressures of T_2 and T_4 composites at 473 K are almost the same. However, in the region where the amount of H_2 desorption is between 0 and 1.2 wt% (2 hydrogen atoms), the dehydrogenation curves of T_2 and T_4 at the higher pressure show certain differences (see the insert figure), *i.e.*, there is a higher pressure slope of the T_2 ($2Mg(NH_2)_2$–3LiH–$LiBH_4$) composite than T_4 ($2Mg(NH_2)_2$–3LiH–1/3$LiBH_4$) composite [36]. The sloping curve indicates that the constitution of the material changes along with the hydrogen desorption. T_2 samples with different amount of hydrogen desorption are characterized by means of X-ray diffraction (XRD), Fourier transform infrared spectroscopy (FTIR), and magic angle spinning nuclear magnetic resonance (MAS NMR).

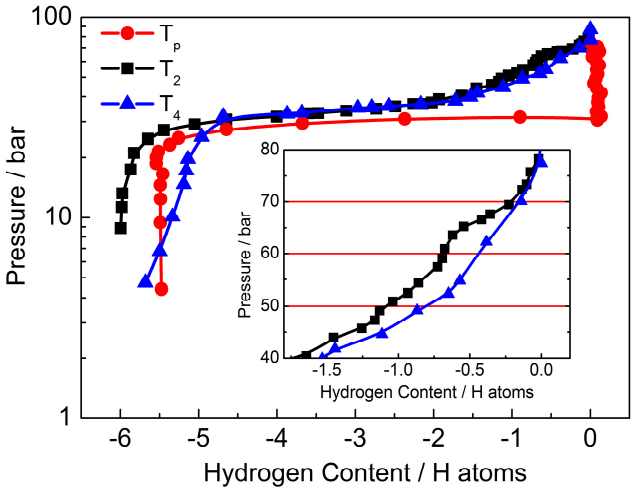

Figure 5. Dehydrogenation Pressure–Composition–Isotherm (PCI) curves of $2Mg(NH_2)_2$–3LiH (T_p), $2Mg(NH_2)_2$–3LiH–$LiBH_4$ (T_2) and $2Mg(NH_2)_2$–3LiH–1/3$LiBH_4$ (T_4) composite at 473 K. The inset is the PCI curves at H/(mol of T_2 and T_4): 0 to 2.

XRD patterns of T_2 after ball milling and desorbing different amount of hydrogen at 460 K are showed in Figure 6, the pattern of fresh-made sample confirms the presence of starting materials $Mg(NH_2)_2$, LiH and $LiBH_4$. When T_2 desorbs 0.25 wt% hydrogen, the peaks of $LiBH_4$ disappear and new peaks assignable to $Li_4BN_3H_{10}$ are visible. As the amount of desorption is up to 0.58 wt%, peaks belonging to Li_2BNH_6 and $Li_4BN_3H_{10}$ appear at the same time. However, with the increasing amount of released hydrogen, the peaks of $Li_4BN_3H_{10}$ become stronger, the peaks of Li_2BNH_6 are getting weaker and finally disappear upon 1.4 wt% hydrogen is desorbed. Because diffraction peaks of Li_2BNH_6 are weak and some of them are overlapped with those of $Li_4BN_3H_{10}$, FTIR are preformed synchronously.

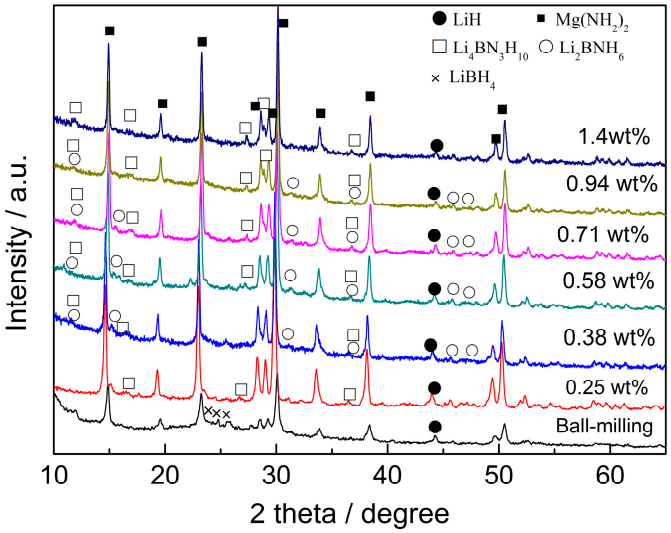

Figure 6. XRD patterns of T_2 ($2Mg(NH_2)_2$–$3LiH$–$LiBH_4$) samples collected at 460 K at different degree of dehydrogenation: 0 wt%, ball-milling stage; 0.25 wt%; 0.38 wt%; 0.58 wt%; 0.71 wt%; 0.94 wt%; and 1.4 wt%.

FTIR spectra of N–H stretching vibrations from the corresponding samples are shown in Figure 7. The B–H stretching frequencies (vibrations from 2000 to 2600 cm^{-1}) were also investigated (Figure S2), but due to the sensitivity of the equipment of FT-IR, there is not much useful information that can be gained. In Figure 7, the post-milled composite gives typical N–H stretching vibrations at 3327 and 3273 cm^{-1} assigned to $Mg(NH_2)_2$, which means $Mg(NH_2)_2$ does not react with $LiBH_4$ during the ball milling process. During the PCI dehydrogenation, $LiNH_2$ produced by Reaction (1) is immediately combined with the nearby $LiBH_4$, which causes that the typical N–H stretching vibrations at 3301 and 3258 cm^{-1} assigned to $LiNH_2$ are not observed. Furthermore, the spectral signals at 3243 and 3301 cm^{-1}, which are assigned to the characteristic vibrations of $Li_4BN_3H_{10}$, suggest that $LiNH_2$ reacts with $LiBH_4$ to form $Li_4BN_3H_{10}$ at the beginning of PCI dehydrogenation. It is likely that the $LiNH_2$–$LiBH_4$ interface reaction produces the Li_2BNH_6 layer and $Li_4BN_3H_{10}$ layer. However, the possibility of melting and decomposition of Li_2BNH_6 to $Li_4BN_3H_{10}$ and $LiBH_4$ may also exist during the PCI measures. The vibrations at 3246 cm^{-1} and 3294 cm^{-1} assigned to Li_2BNH_6 appear after the dehydrogenation of 0.58 wt%, which corresponds well with the XRD measurement. The solid-state phase of Li_2BNH_6 may originate from the quenching of the melts. The vibrations of Li_2BNH_6 are generally weak and broad, and companied with those of $Li_4BN_3H_{10}$. Li_2BNH_6 finally disappears upon desorption of 1.4 wt% hydrogen. We tentatively propose that the formation of Li_2BNH_6 and $Li_2Mg_2(NH)_3$ might be the reason for the high pressure slope in the initial dehydrogenation step.

As shown in Figure 8, ^{11}B MAS NMR spectra of T_2 samples at the different dehydrogenation degree can be fitted into three species, *i.e.*, $LiBH_4$ (−41.62 ppm), $Li_4BN_3H_{10}$ (−39.81 ppm) and Li_2BNH_6 (−37.88 ppm). Figure 8a shows that the peak of ^{11}B signal gradually becomes asymmetric and shifts to the lower chemical shift in pace with the increasing degree of dehydrogenation of T_2 sample. After the weight loss of hydrogen reached 0.58 wt%, the board peak starts to appear the signal of Li_2BNH_6 (−37.88 ppm), which exhibits strongest intensity when desorption weight of hydrogen comes up to 0.94 wt%, plotted in Figure 8b. To summarize the tendency of the peak shift, Figure 8c reveals that the signal area of $Li_4BN_3H_{10}$ increases and the signal peak of $LiBH_4$ decreases with the dehydrogenation.

The signal of Li_2BNH_6 can be distinguished upon releasing 0.58 wt% hydrogen and it soon becomes invisible upon releasing 1.4 wt% hydrogen, which is consistent with the findings of XRD and FT-IR results.

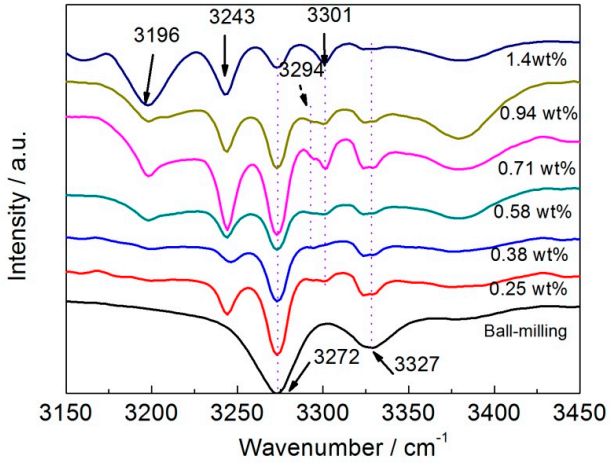

Figure 7. FT-IR spectra of N–H stretching vibrations from T2 ($2Mg(NH_2)_2$–$3LiH$–$LiBH_4$) samples collected at 460 K at different degree of dehydrogenation: 0 wt%, ball-milling stage; 0.25 wt%; 0.38 wt%; 0.58 wt%; 0.71 wt%; 0.94 wt%; and 1.4 wt%.

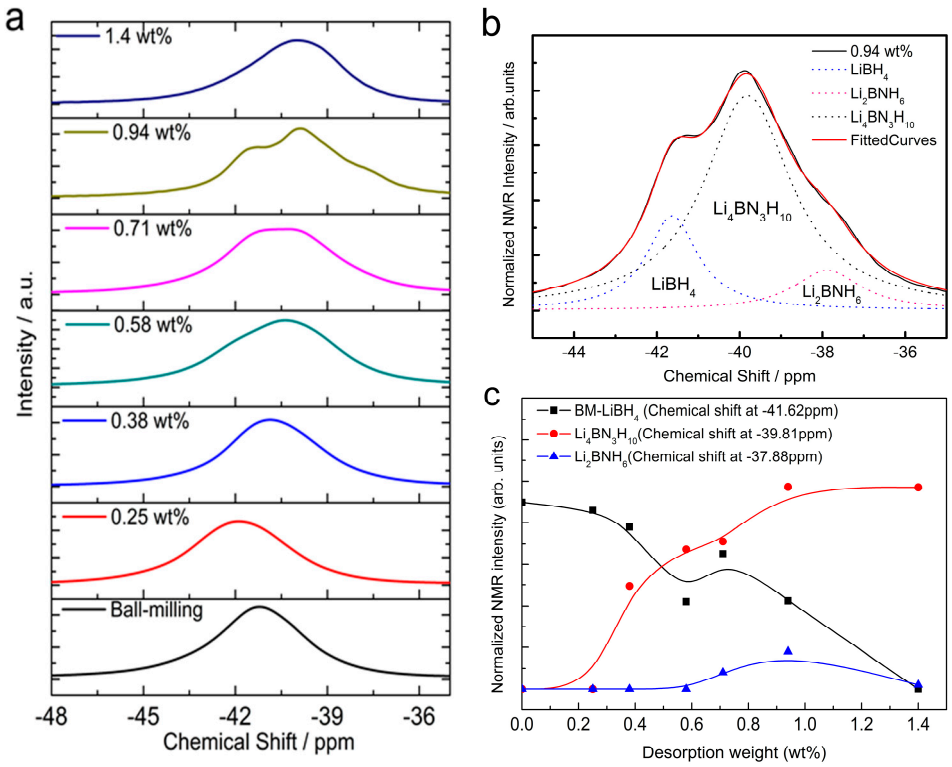

Figure 8. (**a**) ^{11}B magic angle spinning (MAS) NMR spectra of T2 ($2Mg(NH_2)_2$–$3LiH$–$LiBH_4$) samples collected at 460 K at different degree of dehydrogenation: fresh-made, 0.25 wt%, 0.38 wt%, 0.58 wt%, 0.71 wt%, 0.94 wt%, and 1.4 wt%; (**b**) hydrogen desorption fitted NMR spectra of Figure 8a (0.94 wt%) in comparison with $LiBH_4$, Li_2BNH_6 and $Li_4BN_3H_{10}$; and (**c**) the normalized ^{11}B magic angle spinning (MAS) NMR peak intensities of $LiBH_4$ (−41.62 ppm), Li_2BNH_6 (−37.88 ppm) and $Li_4BN_3H_{10}$ (−39.81 ppm) in samples with different degree of hydrogen desorption.

Based on above analyses, the reaction of equimolar $LiNH_2$ and $LiBH_4$ is very likely to happen during the high-pressure slope of T_2 sample. The melted $LiNH_2$–$LiBH_4$ is cooled to room temperature, where $Li4BN_3H_{10}$, $LiBH_4$, and a small amount of solid Li_2BNH_6 can be found [39]. The existence of melted $LiNH_2$–$LiBH_4$ may result in a higher desorption pressure. Future work is still needed to make the mechanism clear.

3. Experimental Section

Lithium hydride (LiH, 99%) (Alfa Aesar, Ward Hill, MA, USA) and Lithium borohydride ($LiBH_4$, 95%) (Sigma Aldrich Fine Chemicals, St. Louis, MO, USA) were used without further purification. Magnesium amide ($Mg(NH_2)_2$) was synthesized by reacting metallic Mg powder (99%, Sigma) with NH_3.

A Retsch PM400 planetary (Haan, Germany) mill was used to ball mill the mixtures of $Mg(NH_2)_2$, LiH and $LiBH_4$ with different molar ratios, such as 2:3:1 and 2:3:1/3 (abbreviated as T_2 and T_4) at 200 rpm for 36 h. Pristine $2Mg(NH_2)_2$–3LiH composite (short for T_p) without additives was also prepared under the same conditions for comparison. $Li_2Mg_2(NH)_3$ was synthesized by heating post-milled $Mg(NH_2)_2$–LiH composite under vacuum for 24 h. Moreover, Li_2BNH_6 was synthesized by ball-milling the mixture of $LiBH_4$ and $LiNH_2$ with the same molar number for 24 h under the atmosphere of argon. To avoid oxygen and moisture contaminations, all the sample loadings were conducted inside a glove box that was filled with purified argon (O_2 < 10 ppm, H_2O < 0.1 ppm).

Thermal decomposition properties of samples were carried on a custom-built temperature programmed desorption (TPD)-mass spectrometer (MS, Hiden Analytical Limited, Warrington, UK) combined system. About 10 mg sample was tested each time at a ramping rate of 2 °C/min. H_2 and NH_3 signals were detected at the *m*/*z* ratios of 2 and 15, respectively. Thermogravimetry coupled differential thermal analysis (TG-DTA) measurements were conducted on a STA-449C (Netzsch, Wittelsbacherstraße, Germany), which was installed in the glove box as mentioned above. The heating rate was 2 °C/min and Ar was the carrier gas.

Pressure–Composition–Isotherm (PCI) measurements and dehydrogenation/hydrogenation experiments were carried out on an automatic Sieverts-type apparatus (Hy-Energy scientific instruments PCT pro-2000, Newark, CA, USA). A sample of *ca.* 200 mg was used each time. Initial pressures in the sample chamber for dehydrogenation and re-hydrogenation experiments were 0.01 and 6 Mpa, respectively.

Isothermal dehydrogenation and re-hydrogenation experiments were carried out on an automatic Sieverts-type apparatus (Advanced Materials Co., PCT, Pittsburgh, PA, USA). Initial pressure in sample chamber for hydrogen desorption was 0.01 MPa, and for absorption was 6 MPa.

Powder X-ray diffraction (XRD) patterns were recorded over a 2θ range of 5°–80° on an X'Pert Pro diffractometer (PANalytical, Almelo, The Netherlands) with Kα radiation at 40 kV and 40 mA. The powder was placed on a self-made cell sealed with an air-tight hood. Fourier transform IR (FTIR) measurements were conducted on a Varian 3100 unit in DRIFT mode to detect the N–H vibration for metal amides or imides. Solid-state ^{11}B nuclear magnetic resonance (NMR) measurements were conducted on a Bruker Advance III 500 NMR spectrometer (Berlin, Germany) with a 4 mm MAS NMR probe working at a frequency of 128.28 MHz.

4. Conclusions

Increasing $LiBH_4$ amount in the $2Mg(NH_2)_2$–3LiH composite leads to a higher dehydrogenation pressure in the slope region. The reason for this change may be due to the melted reaction of $LiNH_2$–$LiBH_4$. Moreover, the kinetics of $2Mg(NH_2)_2$–3LiH–$LiBH_4$ composite are significantly improved in comparison with pristine $2Mg(NH_2)_2$–3LiH sample. Especially, it desorbs *ca.* 80% hydrogen in 100 min and re-hydrogenates 80% hydrogen in 50 min isothermally at 416 K, which is *ca.* 2 times and 18 times as fast as those of $2Mg(NH_2)_2$–3LiH composite.

Supplementary Materials

Supplementary materials can be accessed at: http://www.mdpi.com/1996-1073/8/7/6898/s1.

Acknowledgments

We acknowledge financial support from the project of National Natural Science Funds for Distinguished Young Scholar (51225206), projects of National Natural Science Foundation of China (Grant Nos 21273229, U1232120, 51301161, 21473181 and 51472237) and CAS-Helmholtz Association Collaborative Funding.

Author Contributions

Han Wang conceived and designed the experiments; Han Wang and Hujun Cao performed the experiments; Han Wang, Ping Chen and Guotao Wu analyzed the data; Teng He and Guotao Wu contributed analysis tools; Han Wang wrote the paper; Guotao Wu and Ping Chen revised it critically for intellectual content; Guotao Wu is the person for final approval of the version to be published.

Conflicts of Interest

The authors declare no conflict of interest.

References

1. Schlapbach, L.; Zuttel, A. Hydrogen-storage materials for mobile applications. *Nature* **2001**, *414*, 353–358.
2. Chen, P.; Zhu, M. Recent progress in hydrogen storage. *Mater. Today* **2008**, *11*, 36–43.
3. Bogdanovic, B.; Schwickardi, M. Ti-doped alkali metal aluminium hydrides as potential novel reversible hydrogen storage materials. *J. Alloy. Compd.* **1997**, *253*, 1–9.
4. Chen, J.; Kuriyama, N.; Xu, Q.; Takeshita, H.T.; Sakai, T. Reversible hydrogen storage via titanium-catalyzed $LiAlH_4$ and Li_3AlH_6. *J. Phys. Chem. B* **2001**, *105*, 11214–11220.
5. Fichtner, M.; Fuhr, O.; Kircher, O. Magnesium alanate—A material for reversible hydrogen storage. *J. Alloy. Compd.* **2003**, *356*, 418–422.
6. Chlopek, K.; Frommen, C.; Leon, A.; Zabara, O.; Fichtner, M. Synthesis and properties of magnesium tetrahydroborate, $Mg(BH_4)_2$. *J. Mater. Chem.* **2007**, *17*, 3496–3503.

7. Miwa, K.; Aoki, M.; Noritake, T.; Ohba, N.; Nakamori, Y.; Towata, S.; Zuttel, A.; Orimo, S. Thermodynamical stability of calcium borohydride $Ca(BH_4)_2$. *Phys. Rev. B* **2006**, *74*, doi:10.1103/PhysRevB.74.155122.
8. Zuttel, A.; Rentsch, S.; Fischer, P.; Wenger, P.; Sudan, P.; Mauron, P.; Emmenegger, C. Hydrogen storage properties of $LiBH_4$. *J. Alloy. Compd.* **2003**, *356*, 515–520.
9. Chen, P.; Xiong, Z. Metal–N–H systems for the hydrogen storage. *Scr. Mater.* **2007**, *56*, 817–822.
10. Chen, P.; Xiong, Z.T.; Luo, J.Z.; Lin, J.Y.; Tan, K.L. Interaction of hydrogen with metal nitrides and imides. *Nature* **2002**, *420*, 302–304.
11. Luo, W. ($LiNH_2$–MgH_2): A viable hydrogen storage system. *J. Alloy. Compd.* **2004**, *381*, 284–287.
12. Nakamori, Y.; Kitahara, G.; Orimo, S. Synthesis and dehydriding studies of Mg–N–H systems. *J. Power Sources* **2004**, *138*, 309–312.
13. Xiong, Z.; Wu, G.; Hu, J.J.; Chen, P. Ternary imides for hydrogen storage. *Adv. Mater.* **2004**, *16*, 1522–1525.
14. Wu, H. Structure of ternary imide $Li_2Ca(NH)_2$ and hydrogen storage mechanisms in amide–hydride system. *J. Am. Chem. Soc.* **2008**, *130*, 6515–6522.
15. Xiong, Z.; Wu, G.; Hu, J.; Liu, Y.; Chen, P.; Luo, W.; Wang, J. Reversible hydrogen storage by a Li–Al–N–H complex. *Adv. Funct. Mater.* **2007**, *17*, 1137–1142.
16. Hino, S.; Ichikawa, T.; Leng, H.Y.; Fujii, H. Hydrogen desorption properties of the Ca–N–H system. *J. Alloy. Compd.* **2005**, *398*, 62–66.
17. Hu, J.; Liu, Y.; Wu, G.; Xiong, Z.; Chen, P. Structural and compositional changes during hydrogenation/dehydrogenation of the Li–Mg–N–H system. *J. Phys. Chem. C* **2007**, *111*, 18439–18443.
18. Leng, H.; Ichikawa, T.; Fujii, H. Hydrogen storage properties of Li–Mg–N–H systems with different ratios of $LiH/Mg(NH_2)_2$. *J. Phys. Chem. B* **2006**, *110*, 12964–12968.
19. Luo, W.; Wang, J.; Stewart, K.; Clift, M.; Gross, K. Li–Mg–N–H: Recent investigations and development. *J. Alloy. Compd.* **2007**, *446*, 336–341.
20. Xiong, Z.T.; Wu, G.T.; Hu, J.J.; Chen, P.; Luo, W.F.; Wang, J. Investigations on hydrogen storage over Li–Mg–N–H complex—The effect of compositional changes. *J. Alloy. Compd.* **2006**, *417*, 190–194.
21. Chen, X.Y.; Guo, Y.H.; Yu, X.B. Enhanced dehydrogenation properties of modified $Mg(NH_2)_2$–$LiBH_4$ composites. *J. Phys. Chem. C* **2010**, *114*, 17947–17953.
22. Noritake, T.; Aoki, M.; Towata, S.; Ninomiya, A.; Nakamori, Y.; Orimo, S. Crystal structure analysis of novel complex hydrides formed by the combination of $LiBH_4$ and $LiNH_2$. *Appl. Phys. A* **2006**, *83*, 277–279.
23. Weidner, E.; Dolci, F.; Hu, J.J.; Lohstroh, W.; Hansen, T.; Bull, D.J.; Fichtner, M. Hydrogenation reaction pathway in $Li_2Mg(NH)_2$. *J. Phys. Chem. C* **2009**, *113*, 15772–15777.
24. Li, C.; Liu, Y.F.; Gu, Y.J.; Gao, M.X.; Pan, H.G. Improved hydrogen-storage thermodynamics and kinetics for an RbF-doped $Mg(NH_2)_2$–2LiH system. *Chem.Asian J.* **2013**, *8*, 2136–2143.
25. Liang, C.; Liu, Y.F.; Gao, M.X.; Pan, H.G. Understanding the role of K in the significantly improved hydrogen storage properties of a KOH-doped Li–Mg–N–H system. *J. Mater. Chem. A* **2013**, *1*, 5031–5036.

26. Liu, Y.F.; Li, C.; Li, B.; Gao, M.X.; Pan, H.G. Metathesis reaction-induced significant improvement in hydrogen storage properties of the KF-added $Mg(NH_2)_2$–2LiH system. *J. Phys. Chem. C* **2013**, *117*, 866–875.
27. Wang, J.H.; Liu, T.; Wu, G.T.; Li, W.; Liu, Y.F.; Araujo, C.M.; Scheicher, R.H.; Blomqvist, A.; Ahuja, R.; Xiong, Z.T.; *et al*. Potassium-modified $Mg(NH_2)_2$/2 LiH system for hydrogen storage. *Angew. Chem. Int. Ed.* **2009**, *48*, 5828–5832.
28. Hu, J.J.; Fichtner, M.; Chen, P. Investigation on the properties of the mixture consisting of $Mg(NH_2)_2$, LiH, and $LiBH_4$ as a hydrogen storage material. *Chem. Mater.* **2008**, *20*, 7089–7094.
29. Hu, J.J.; Liu, Y.F.; Wu, G.T.; Xiong, Z.T.; Chua, Y.S.; Chen, P. Improvement of hydrogen storage properties of the Li–Mg–N–H system by addition of $LiBH_4$. *Chem. Mater.* **2008**, *20*, 4398–4402.
30. Durojaiye, T.; Hayes, J.; Goudy, A. Rubidium hydride: An exceptional dehydrogenation catalyst for the lithium amide/magnesium hydride system. *J. Phys. Chem. C* **2013**, *117*, 6554–6560.
31. Yang, J.; Sudik, A.; Siegel, D.J.; Halliday, D.; Drews, A.; Carter, R.O., 3rd; Wolverton, C.; Lewis, G.J.; Sachtler, J.W.; Low, J.J.; *et al*. A self-catalyzing hydrogen-storage material. *Angew. Chem. Int. Ed.* **2008**, *47*, 882–887.
32. Li, B.; Liu, Y.F.; Gu, J.; Gao, M.X.; Pan, H.G. Synergetic effects of *in situ* formed CaH_2 and $LiBH_4$ on hydrogen storage properties of the Li–Mg–N–H system. *Chem. Asian J.* **2013**, *8*, 374–384.
33. Li, B.; Liu, Y.F.; Gu, J.; Gu, Y.J.; Gao, M.X.; Pan, H.G. Mechanistic investigations on significantly improved hydrogen storage performance of the $Ca(BH_4)_2$-added $2LiNH_2/MgH_2$ system. *Int. J. Hydrog. Energy* **2013**, *38*, 5030–5038.
34. Pan, H.G.; Shi, S.B.; Liu, Y.F.; Li, B.; Yang, Y.J.; Gao, M.X. Improved hydrogen storage kinetics of the Li–Mg–N–H system by addition of $Mg(BH_4)_2$. *Dalton Trans.* **2013**, *42*, 3802–3811.
35. Li, B.; Liu, Y.F.; Li, C.; Gao, M.X.; Pan, H.G. *In situ* formation of lithium fast-ion conductors and improved hydrogen desorption properties of the $LiNH_2$–MgH_2 system with the addition of lithium halides. *J. Mater. Chem. A* **2014**, *2*, 3155–3162.
36. Cao, H.J.; Wu, G.T.; Zhang, Y.; Xiong, Z.T.; Qiu, J.S.; Chen, P. Effective thermodynamic alteration to $Mg(NH_2)_2$–LiH system: Achieving near ambient-temperature hydrogen storage. *J. Mater. Chem. A* **2014**, *2*, 15816–15822.
37. Chater, P.A.; David, W.I.F.; Anderson, P.A. Synthesis and structure of the new complex hydride $Li_2BH_4NH_2$. *Chem. Commun.* **2007**, *45*, 4770–4772.
38. Wu, H.; Zhou, W.; Udovic, T.J.; Rush, J.J.; Yildirim, T. Structures and crystal chemistry of Li_2BNH_6 and $Li_4BN_3H_{10}$. *Chem. Mater.* **2008**, *20*, 1245–1247.
39. Borgschulte, A.; Jones, M.O.; Callini, E.; Probst, B.; Kato, S.; Zuttel, A.; David, W.I.F.; Orimo, S. Surface and bulk reactions in borohydrides and amides. *Energy Environ. Sci.* **2012**, *5*, 6823–6832.
40. Matsuo, M.; Remhof, A.; Martelli, P.; Caputo, R.; Ernst, M.; Miura, Y.; Sato, T.; Oguchi, H.; Maekawa, H.; Takamura, H.; *et al*. Complex hydrides with $(BH_4)^-$ and $(NH_2)^-$ anions as new lithium fast-ion conductors. *J. Am. Chem. Soc.* **2009**, *131*, 16389–16391.